Proceedings of the Estonian Academy of Sciences,
2022, **71**, 3, 221–226
https://doi.org/10.3176/proc.2022.3.03
Available online at www.eap.ee/proceedings

TISSUE OPTICS AND SPECTROSCOPY

Effective attenuation coefficient and penetration depth of 630 nm laser light in polyvinyl alcohol slime glue phantoms simulating the human brain tumour

Lindokuhle Ntombela, Naven Chetty* and Bamise Adeleye

School of Chemistry and Physics, University of KwaZulu–Natal, Private Bag X01, Scottsville 3209, South Africa

Received 22 November 2021, accepted 18 March 2022, available online 3 August 2022

Abstract. The effectiveness of optical methods such as photodynamic therapy (PDT) depends on the amount of light distribution within the tissue to aid their potential for early cancer detection in a quantitative and non-invasive manner. Knowledge of the effective attenuation coefficient and penetration depth for the laser light is crucial to ensuring that the tumour tissue receives adequate optical energy. This study investigated the effective attenuation coefficient and penetration depth of He–Ne 630 nm red laser light in polyvinyl alcohol slime glue phantoms simulating human brain tumour tissues. The effective attenuation coefficient (μ_{eff}) and penetration depth (δ) were deduced from the absorption coefficient (μ_a), scattering coefficient (μ_s), and anisotropy factor (g) obtained from the Henyey–Greenstein (H–G) function by collimated laser beam measurements. We found that the effective attenuation coefficient and penetration depth were 0.25 ± 0.02 mm^{-1} and 4.00 mm, respectively, in the simulated phantoms. These values were in reasonable agreement with values reported for malignant human brain tumour tissues in the literature. The constructed phantoms would be an excellent tool for the continued evaluation of PDT as an essential therapeutic procedure in cancer management.

Keywords: biomedical physics, slime phantoms, effective attenuation coefficient, penetration depth, He–Ne laser.

1. INTRODUCTION

An accurate and early diagnosis of cancerous tissue is a crucial factor in reducing mortality and management costs. Cancer cells multiply uncontrollably to crowd healthy areas of the affected tissue, thereby forming a tumour lump. Brain tumours known as intracranial tumours occur when brain cells show abnormal growth ranging from benign to malignant and eventually metastatic [1].

Biomedical imaging techniques have emerged as a useful resource in all phases of cancer management, including screening, detection, staging, and treatment [2,3]. Existing imaging modalities to have shown great capabilities for cancer cells are positron emission tomography (PET), computed tomography (CT), magnetic resonance imaging (MRI), and optical imaging [4–8]. Several contrast mechanisms for differentiating normal from pathological processes and tissues in optical imaging with relatively simple instrumentation and speed have raised interest in the technology [9,10]. Laser light interaction with tissues involves attenuation and penetration of light as a function of absorption and scattering properties. These optical properties are utilized to obtain biochemical and morphological information about specific cells [3,9]. However, it is still challenging to accurately heat a deep-seated tumour, such as a malignant brain tumour, with appropriate power intensity [11]. The probability that an interaction will occur when photon energy passes through a target tissue depends on the

* Corresponding author, chettyn3@ukzn.ac.za

tissue's energy, composition, and thickness [12], the magnitude of which varies for different tissues. Measurements employing a phantom with appropriate optical properties for the desired tumour tissue are essential to thoroughly estimate the amount of laser light needed to heat a tumour [11]. Phantoms mimicking the brain tumour should be of non-toxic materials, practical imaging applications – specifically ultrasound attenuation and CT contrast. Such optical phantoms must also have important vital properties such as durability, and similar mechanical behaviour to the human tissue so that it can be handled and used repeatedly [13,14]. The phantom slime material considered for this study was formulated by mixing polyvinyl alcohol (PVA) slime glue with natural borax powder [$Na_2B_4O_7 \cdot 10H_2O$]. After mixing the substances, the effective chemical component in borax cross-linked the polyvinyl acetate molecules in the glue to form the viscoelastic slime [15].

A major advantage of PVA based phantoms is their superior mechanical properties, which are readily adjustable over the range found in the tissue by modifying its freeze-thaw cycles [13,14]. They show good optical transparency, a high degree of elasticity, lower surface friction resistance suitable for applications such as blood vessel biomodelling, as well as good acoustic and durability properties [13, 16–17].

A considerable number of studies on PVA slime glue based phantoms have already been performed with valuable results. Hebden et al. [15] presented a novel design of highly compressible phantoms for diffuse optical tomography, with polyvinyl alcohol slime as the principal component mixed with scattering or absorbing agents for reproducible optical properties. They established that phantoms of arbitrary size and shape might be produced by containing the slime within a thin latex shell with constant properties for at least three months [15]. The effect of poly(ethylene oxide) (PEO) on the mechanical properties of PVA/borax gels and the capability to retain and improve interactions with miscible organic solvents in conservation applications was investigated by Riedo et al. [18]. The addition of PEO to the PVA/borate dispersion modifies the viscoelastic behaviour and liquid phase retention of the gels, increasing the apparent gel relaxation time, stability of the dispersions, and their ability to maintain the shape after use. Yusoff et al. [19] investigated the homogeneity and stability of the poly(vinyl alcohol) slime phantom and its suitability and potential as MRI phantom. The results were promising as the signal-to-noise ratio (SNR), T1, and T2 values of the fabricated phantoms were stable over time and in good agreement with the average values of human tissues.

This study designed and developed PVA slime phantom tissues to determine the effective attenuation coefficient and optical penetration depth compatible with values reported for a malignant human brain tumour at 630 nm. Low-power red light (emitting 630 nm) is regularly employed for tumour destruction following oral or intravenous administration of a photosensitizing drug in photodynamic therapy (PDT). For correct dosimetry, it is essential to evaluate the penetration depths of tissues with phantom materials with relative ease of fabrication and controllable properties with regard to real tissues.

2. MATERIALS AND METHODS

2.1. Phantom composition and recipe

The phantoms were prepared with poly(vinyl alcohol) slime glue (Locally Yours Shop, South Africa), borax powder (sodium tetraborate decahydrate) (Allied Drug Company, South Africa), and India ink (PRO-4100, Pro Art). The fabrication process involved the following steps:

- 3 g of borax powder [$Na_2B_4O_7 \cdot 10H_2O$] was dissolved in a beaker containing 50 mL of deionized water. The borax solution was stirred vigorously on a hot plate with a magnetic stirrer until it reached 70 °C to dissolve the powder granules completely.
- The powder appearance changed from murky to crystal clear, indicating that the borax powder was utterly dissolved, and the solution was uniformly distributed at this temperature.
- The borax solution was allowed to cool to about 20 °C while 100 mL of PVA slime glue was prepared in a second beaker.
- Absorption properties were induced by adding 0.4 mL of India ink while the borax solution was gradually added using a 20 ml syringe, and the solution was gently stirred with a wooden rod.
- The India ink (PRO-4100, Pro Art) was added slowly to increase the internal absorption of the slime phantom.
- The slime phantom was formed when the borax was completely diffused with the PVA glue chains. The fabricated phantom was then subjected to shear stress for brittleness.
- Lastly, the slime phantom was filled into a beaker, wrapped with foil, and placed in a refrigerator overnight to allow for a full cross-link and prevent extreme changes in temperature and humidity.
- During the heating process, the temperature of the sample was monitored using a Techgear TG732TK dual channel digital thermometer modified to utilize a thermocouple attached to the reverse side of a Velcro strap. The digital thermocouple strapped around the beaker provides accurate temperature measurements of the heated solution within the accuracy of ± 5 °C.

2.2. Measurements of optical properties

The red laser wavelength of 630 nm was incident on slices of the phantom sample with the beam positioned at a fixed distance (0.4 m) from the sample. The samples were mounted on a slice holder perpendicular (0° incidence angles) to the incident light power (P_o), with the transmitted power at an angle (Fig. 1). A 25 mm diameter cube splitter (Edmund Optics, USA) was used to continuously monitor the incident beam power. Measurements of the incident and transmitted laser light power through each slice were obtained by directly compressing thin samples of the slime phantom of various sizes between two optical glasses (n = 1.52), and the actual thickness (L) was measured using a digital vernier calliper. A drop of saline solution was used to improve the optical contact between the tissue and glass, and to minimize rough effects for perfect scattering. The laser source powers were estimated in mW using an EO 54-018 collimated digital handheld laser power metre with a response time of 2 to 10 ms (Edmund Optics, USA).

The singly unscattered light relative to the normal line was detected by the ray optics technique. The scattering angle was measured with a goniometer since the light is mostly forward scattered (anisotropy scattering) [20]. All measurements were performed at room temperature.

The total attenuation coefficient (μ_t) was computed from the Lambert–Beer law (Eq. 1), assuming that multiple scattering does not occur:

$$\mu_t = -\frac{1}{L}\ln\left[\frac{P}{P_o}\right], \tag{1}$$

where L is the sample thickness, P_o the power of the incident beam, and P denotes the power of the transmitted light.

A graph of - In $\left[\frac{P}{P_o}\right]$ versus thickness L was plotted for each phantom-sample tissue, and the attenuation coefficient μ_t is represented by the slope of the linear fit.

In a turbid medium, the attenuation coefficient is also described as the sum of the absorption and scattering coefficients as:

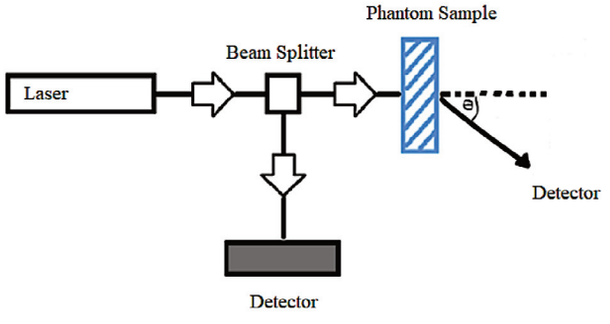

Fig. 1. Set-up for the measurement of optical properties.

$$\mu_t = \mu_a + \mu_s. \tag{2}$$

The effective attenuation coefficient (μ_{eff}) and penetration depth (δ) were deduced from the absorption coefficient (μ_a), scattering coefficient (μ_s), and anisotropy factor (g).

The anisotropy factor g was computed using the Henyey–Greenstein (H–G) phase function (Eq. 3) valid within the limits of single scattering, wherein the dependence of the exit angle on the transmitted intensity is expressed as [21]:

$$P(\theta) = \mathbf{K}\left[\frac{1-g^2}{(1+g^2-2g\cos\theta)^{\frac{3}{2}}}\right]. \tag{3}$$

This information allowed for the evaluation of the effective attenuation coefficient as follows:

$$\mu_{eff} = \sqrt{3\mu_a\,[\mu_a + (1-g)\mu_s]}. \tag{4}$$

The reciprocal of the effective attenuation coefficient provides an estimation of the penetration depth:

$$\delta = \frac{1}{\mu_{eff}}. \tag{5}$$

3. RESULTS AND DISCUSSION

In this study, PVA slime glue phantoms were developed to determine the effective attenuation coefficient and optical penetration depth of the 630 nm laser light in grade III malignant brain tumour tissues, as found in the literature. Tables 1 and 2 present the incident and transmitted laser power intensities through different thicknesses of the pure phantom and the samples with added absorption. The range of optical thicknesses (L) was tested in this experiment, and $L \leq 3$ mm showed significantly negligible effects of multiple scattering. The pure phantom scattered the light beam at small angles (< 10°) measured with a goniometer. The anisotropy factor values, computed from Eq. 3 using Wolfram Mathematica applied only to the pure scattering samples, were typical of cancerous tissues for visible light wavelengths [22]. Each value reported is the average of four repeated measurements of the thickness of each slice.

Figs 2 and 3 show the graph of - In $\left[\frac{P}{P_o}\right]$ plotted as a function of thickness for all phantom samples, with error bar plots showing the standard deviation of uncertainty. The total attenuation coefficient corresponds to the slope of the linear fit. The statistical measure ($R^2 \approx 1$) for the overall samples indicated a robust correlation between the values of - In $\left[\frac{P}{P_o}\right]$ and L. Therefore, increasing the incident intensities with large thicknesses will be an effective way to deliver adequate light into deeper areas of the tumour tissue.

Table 1. Power intensities of the 630 nm laser through a mixture of 60 g/L concentration of borax and 100 mL of PVA slime glue

Sample thickness (mm)	Incident power (mW)	Transmitted power (mW)	$-\ln\left[\frac{P}{P_o}\right]$	θ	g
0.53	4.46	3.27	0.311	4	0.993
1.01	4.18	2.83	0.390	4.8	0.989
1.52	4.81	2.39	0.700	6	0.982
2.04	4.94	1.96	0.925	7	0.977
2.50	4.60	1.61	1.051	8	0.973
3.02	4.72	1.19	1.380	9.5	0.966

Table 2. Power intensities of the 630 nm laser through 60 g/L of borax with 100 mL of slime glue, and 0.4 mL of India ink to assess the effects of added absorbers on the total attenuation coefficients

Sample thickness (mm)	Incident power (mW)	Transmitted power (mW)	$-\ln\left[\frac{P}{P_o}\right]$
0.49	4.03	2.89	0.333
1.03	4.21	2.34	0.588
1.52	4.39	1.89	0.830
2.01	4.62	1.40	1.195
2.56	4.58	1.07	1.453
3.11	4.67	0.71	1.888

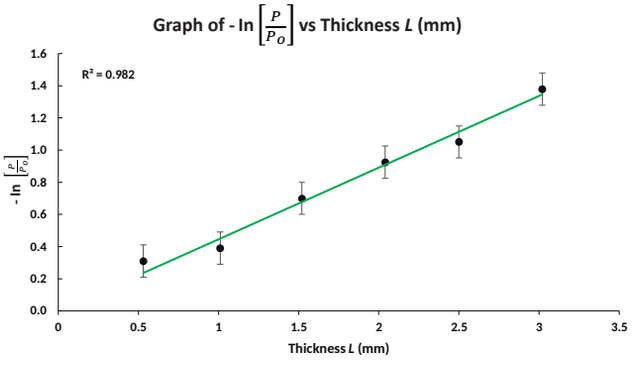

Fig. 2. Logarithmic intensity as a function of thickness with associated linear fit options to determine the total attenuation coefficient for the pure slime phantom at 630 nm.

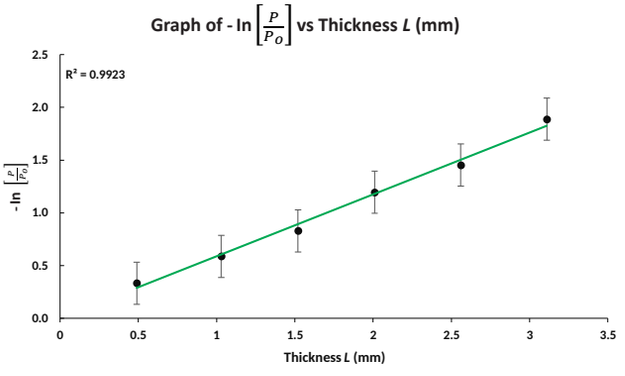

Fig. 3. Logarithmic intensity as a function of thickness with associated linear fit options to determine the total attenuation coefficient for the slime phantom with absorbers at 630 nm.

The phantom's slime material possesses negligible optical absorption properties; hence, the assumption of $\mu_t \approx \mu_s$ was considered for the pure phantom sample and the absorption properties (μ_a) of the ink acted additionally to create the μ_t of the phantom.

The scattering coefficient (μ_s = 0.445 mm^{-1}), anisotropy factor (g = 0.980), reduced scattering coefficient (μ_s = 0.0089 mm^{-1}), and absorption coefficient (μ_a= 0.142 mm^{-1}) were obtained from Eq. 2 considering $\mu_t \approx \mu_s$ for the pure slime phantom sample. These optical properties allowed for the estimation of the effective attenuation coefficient and penetration depth (Table 3).

Despite the relative simplicity of the methodology developed to measure the optical properties, with several approaches taken to minimize artefacts in our study, the results obtained were comparable to reported values in the literature (Table 3). However, Svaasand et al. [25] found lower penetration depth values compared to this study and the studies by Wilson et al. [23], Muller and Wilson [24]. These observed differences may be due to the varying tissue samples, theoretical models employed, and approximations made. The penetration depth was evaluated for five human brains (two neonates and three adults) immediately after autopsies by Svaasand et al. [25], following interstitial irradiation of the tissues. They concluded that the degree of myelination influences the penetration depth, which increases the scattering of light and reduces the diffusion coefficient. The slight variation in values may also be attributed to changes in real issues, such as blood drainage and de-oxygenation with time after resection, or alterations in blood flow or oedema caused by irradiation [23]. Moreover, the tissues were probably a mix of both normal brain matter and tumour.

Discrepancies among the results may also be due to undetectable multiple scattering in our study. This impacted much the transmitted powers and the scattering angles recorded. To satisfy the condition of single scattering, the samples were sliced to a significantly small thickness while maintaining rigidity. Moreover, the distance between the sample holder and the detector was sufficient to reduce the scattering effects on the measurements of optical properties.

Generally, the depth of light penetration into normal tissues is considerably less than in the case of tumorous tissues. Nevertheless, the ability of light-based techniques such as PDT to treat deep-seated pathologies is limited by a significant attenuation in potency as the light penetrates deeper into the tissue [26].

Clinically, the delivery of light into deeper and complex treatment sites is achieved through thin optical fibres that deliver light and simultaneously act as diagnostic sensors to gauge vital PDT parameters, critically impacting the therapeutic response [26].

Table 3. Comparison of the effective attenuation coefficient and penetration depth values obtained in this study and other studies at 630 nm

Brain tumour tissue	μ_{eff} (mm^{-1})	δ (mm)
Present study	0.25 ± 0.02	4.00
[23]	0.24	4.17
[24]	0.22–0.66	1.52–4.55
[25]	0.38–0.588	1.7–2.6

4. CONCLUSIONS

This study confirms that PVA slime glue based phantoms with optical properties evaluating the effective attenuation coefficient and penetration depths of red laser (630 nm) in malignant brain tumour tissues could be fabricated. The repeatability of the recipe was verified and showed the capability to reproduce the desired properties.

Undoubtedly, the developed phantoms can be used in combination with further research to optimize PDT irradiation procedures and establish accurate light dosimetry for brain tumour treatments.

ACKNOWLEDGEMENTS

This work was funded from the research allowance granted to Naven Chetty by the University of KwaZulu–Natal, South Africa. The publication costs of this article were partially covered by the Estonian Academy of Sciences.

REFERENCES

1. Kayode, A. A. A., Shahzadi, A., Akram, M., Anwar, H., Kayode. O. T., Akinnawo, O. O. and Okoh, O. S. Brain tumor: An overview of the basic clinical manifestations and treatment. *Glob. J. Cancer Ther*., 2020, **6**(1), 038–041. https://dx.doi.org/10.17352/2581-5407.000034
2. Fass, L. Imaging and cancer: a review. *Mol. Oncol*., 2008, **2**, 115–152. https://doi.org/10.1016/j.molonc.2008.04.001
3. García-Figueiras, R., Baleato-González, S., Padhani, A. R., Luna-Alcalá, A., Vallejo-Casas, J. A., Sala, E. et al. How clinical imaging can assess cancer biology. *Insights into Imaging*, 2019, **10**(1), 28. https://doi.org/10.1186/s13244-019-0703-0
4. Bailey, D. L., Maisey, M. N., Townsend, D. W., Valk, P. E. and Maisey, M. N. *Positron Emission Tomography*. Springer, London, 2005. https://doi.org/10.1007/b136169

5. Brenner, D. J. and Hall, E. J. Computed tomography – an increasing source of radiation exposure. *N. Engl. J. Med.*, 2007, **357**(22), 2277–2284. https://doi.org/10.1056%2Fnejmra072149
6. Huettel, S. A., Song, A. W. and McCarthy, G. *Functional Magnetic Resonance Imaging*. Sinauer Associates, Sunderland, MA, 2004.
7. Gu, M. *Advanced Optical Imaging Theory*. Springer, Berlin, Heidelberg, 2000. https://doi.org/10.1007/978-3-540-48471-4
8. Hou, L. C., Veeravagu, A., Hsu, A. R. and Tse, V. C. Recurrent glioblastoma multiforme: a review of natural history and management options. *Neurosurg. Focus*, 2006, **20**(4), E5. https://doi.org/10.3171%2Ffoc.2006.20.4.2
9. Solomon, M., Liu, Y., Berezin, M. Y. and Achilefu, S. Optical imaging in cancer research: basic principles, tumor detection, and therapeutic monitoring. *Med. Princ. Pract*., 2011, **20**(5), 397–415. https://doi.org/10.1159%2F000327655
10. Mehrmohammadi, M., Yoon, S. J., Yeager, D. and Emelianov, S. Y. Photoacoustic imaging for cancer detection and staging. *Curr. Mol. Imaging*, 2013, **2**(1), 89–105. https://doi.org/10.2174%2F2211555211302010010
11. Kato, H. and Ishida, T. Development of an agar phantom adaptable for simulation of various tissues in the range 5–40 MHz (Hyperthermia treatment of cancer). *Phys. Med. Biol*., 1987, **32**(2), 221–226. https://doi.org/10.1088%2F0031-9155%2F32%2F2%2F006
12. Hopkins, D. N. *Determination of the linear attenuation coefficients and build-up factors of MCP-96 alloy for use in tissue compensation and radiation protection*. MA thesis. Ball State University, IN, USA, 2010.
13. Mackle, E. C., Shapey, J., Maneas, E., Saeed, S. R., Bradford, R., Ourselin, S. et al. Patient-specific polyvinyl alcohol phantom fabrication with ultrasound and X-ray contrast for brain tumor surgery planning. *J. Vis. Exp*., 2020, **2020**(161), e61344. https://doi.org/10.3791%2F61344
14. Lamouche, G., Kennedy, B. F., Kennedy, K. M., Bisaillon, C. E., Curatolo, A., Campbell, G. et al. Review of tissue simulating phantoms with controllable optical, mechanical and structural properties for use in optical coherence tomography. *Biomed. Opt. Express*, 2012, **3**(6), 1381–1398. https://doi.org/10.1364%2Fboe.3.001381
15. Hebden, J. C., Price, B. D., Gibson, A. P. and Royle, G. A soft deformable tissue-equivalent phantom for diffuse optical tomography. *Phys. Med. Biol*., 2006, **51(**21), 5581–5590. https://doi.org/10.1088%2F0031-9155%2F51%2F21%2F013
16. Guo, K., Zhu, Y., Wang, J., Jiang, C. and Yu, J. Characterizing the viscoelastic properties of a tissue-mimicking phantom for ultrasound elasticity imaging studies. *IOP Conf. Ser.: Mater. Sci. Eng*., 2019, **490**(2), 022035. https://doi.org/10.1088%2F1757-899x%2F490%2F2%2F022035
17. Kosukegawa, H., Mamada, K., Kuroki, K., Liu, L., Inoue, K., Hayase, T. and Ohta, M. Measurements of dynamic viscoelasticity of poly (vinyl alcohol) hydrogel for the development of blood vessel biomodeling. *J. Fluid Sci. Technol*., 2008, **3**(4), 533–543. https://doi.org/10.1299/jfst.3.533
18. Riedo, C., Caldera, F., Poli, T. and Chiantore, O. Poly(vinyl alcohol)-borate hydrogels with improved features for the cleaning of cultural heritage surfaces. *Herit. Sci*., 2015, **3**(23). https://doi.org/10.1186%2Fs40494-015-0053-2
19. Yusoff, A. N., Ding, A. Z., Azman, N., Awang, M. N. A. and Abdul Manan, H. Homogeneity and stability of poly (vinyl alcohol) slime phantom with different borax concentration. *ECS J. Solid State Sci. Technol*., 2019, **27**(1&2), 51–67.
20. Arnfield, M. R., Tulip, J. and McPhee, M. S. Optical propagation in tissue with anisotropic scattering. *IEEE Trans. Biomed. Eng*., 1988, **35**(5), 372–385. https://doi.org/10.1109%2F10.1396
21. Zaccanti, G. and Bruscaglioni, P. Method of measuring the phase function of a turbid medium in the small scattering angle range. *Appl. Opt*., 1989, **28**(11), 2156–2164. https://doi.org/10.1364%2Fao.28.002156
22. Pu, Y., Chen, J. and Wang, W. Investigation of scattering coefficients and anisotropy factors of human cancerous and normal prostate tissues using Mie theory. *SPIE*, 2014, **8941**. https://doi.org/10.1117%2F12.2034863
23. Wilson, B. C., Muller, P. J. and Yanch, J. C. Instrumentation and light dosimetry for intra-operative photodynamic therapy (PDT) of malignant brain tumours. *Phys. Med. Biol*., 1986, **31**(2), 125–133. https://doi.org/10.1088%2F0031-9155%2F31%2F2%2F002
24. Muller, P. J. and Wilson, B. C. An update on the penetration depth of 630 nm light in normal and malignant human brain tissue in vivo. *Phys. Med. Biol*., 1986, **31**(11), 1295–1297. https://doi.org/10.1088%2F0031-9155%2F31%2F11%2F012
25. Svaasand, L. O. and Ellingsen, R. Optical properties of human brain. *Photochem. Photobiol*., 1983, **38**(3), 293–299. https://doi.org/10.1111%2Fj.1751-1097.1983.tb02674.x
26. Mallidi, S., Anbil, S., Bulin, A. L., Obaid, G., Ichikawa, M. and Hasan, T. Beyond the barriers of light penetration: strategies, perspectives and possibilities for photodynamic therapy. *Theranostics*, 2016, **6**(13), 2458–2487. https://doi.org/10.7150%2Fthno.16183